PERIODICA POLYTECHNICA SER. MECH. ENG. VOL. 49, NO. 2, PP. 163–180 (2005)

VALIDATION OF A COMPUTATIONAL FLUID DYNAMICS METHOD TO BE APPLIED TO LINEAR CASCADES OF TWISTED-SWEPT BLADES

Gergely RÁBAI and János VAD

Department of Fluid Mechanics,
Budapest University of Technology and Economics
Bertalan Lajos u. 4 – 6. H–1111 Budapest, Hungary

Received: January 24, 2005

Abstract

A synthetic method has been elaborated for the validation of a Computational Fluid Dynamics tool developed for the future investigation of the combined aerodynamic effects of sweep and spanwise changing stagger angle on stationary linear blade cascades. The validation method is based on specially selected experimental data available in the open technical literature. The capabilities of the CFD method for resolution of near-endwall phenomena due to sweep as well as of the effect of changing incidence were tested. The CFD methodology and the experimental validation process have been documented herein in accordance with the requirements regarding industrial CFD tools.

Keywords: axial flow turbomachinery, stationary linear cascades, computational fluid dynamics, validation, sweep, spanwise changing blade circulation.

1. Introduction

Computational Fluid Dynamics (CFD) is of continuously increasing importance in design, optimization, and performance prediction of axial flow turbomachinery cascades. In order to study certain fluid mechanical phenomena, investigation on stationary linear cascades (SLC) instead of realistic annular stator and rotor blade rows appears often as a widely accepted modelling simplification. This simplification is widespread in survey of effects of blade sweep, in experimental [1]–[3] as well as in CFD [4, 5] projects. An axial flow turbomachinery blade is swept when each blade section of a datum blade of radial stacking line is displaced parallel to the relative flow direction in a prescribed manner. Blade sweep, or circumferential blade skew [6] offer a potential for improvement of turbomachinery stage performance and efficiency, increase of pressure peak, shift of stall margin towards lower flow rate, reduction of shock losses, and noise reduction [7].

All of the above studies are confined to SLC with spanwise constant stagger angle, corresponding to a spanwise nearly constant incidence angle. Nevertheless, the incidence angle often varies along the blade span. This may be due to the controlled vortex rotor design concept [8] (i.e. design blade circulation increasing along the dominant part of span), or due to the off-design operation of blade rows of free vortex design [9] (i.e. spanwise constant design blade circulation).

The above yield that blade sweep and spanwise changing incidence often characterize the axial flow blade rows simultaneously in practical applications. Some examples are: silent low-pressure industrial fans [6], automotive cooling fans of high specific performance [10, 11], low-speed wind tunnel fans [12], high-pressure industrial fans [13], low-speed compressors [14].

As already suggested, no SLC data are available in the open literature on the combined effects of sweep and spanwise changing incidence. In order to investigate such effects on a general platform, development of a reliable CFD methodology applied to SLC of twisted-swept blades is essential. This paper reports on the elaboration and experimental validation of a CFD technique forming the basis for future generation of reliable CFD tools modelling twisted-swept blades. The activity presented herein is a continuation of the validation work documented in [15].

2. Definition of Case Study, Validation Database, and the Related Validation Process

Since no experimental SLC database is available in the open literature related to combined effects of sweep and varying incidence, it is an inevitable compromise to separate these features and to find experimental validation data sets related to
i) SLC of comparative unswept and swept blades tested at a given incidence,
ii) SLC of unswept blades tested at various incidences.

It is obvious that the data sets achieving the goals of i) and ii) must be related to SLC consisting of blades of identical blade profile and having as similar cascade geometry and flow conditions as possible. The most suitable experimental database found by the authors and meeting these demands is the following: [2] (supported by further data in [4, 16] for i, supplemented by [17] for ii). These sources discuss measurements on blades of controlled diffusion profile developed by Sanger [18]. The blades are symmetrical to the midspan section and are bounded by endwalls with no clearance. *Table 1* presents a comparison between the cascade geometrical data in [2] and [17]. The Reynolds numbers – based on the inlet velocity, the blade chord and the kinematic viscosity of air at 20°C – for test cases processed herein are also presented in the table. Although some discrepancy can be observed in the data in *Table 1*, authors judged it reasonable to use [2] and [17] as a consistent validation database. This judgment is to be confirmed by comparison of data available in [2] and [17] for identical (or the possibly closest) experimental situations (see *Fig. 2* later).

Authors refer to the above publications with respect to the measurement technical details.

In [2], detailed measurement data are available for cascades of unswept (straight) blades and of blades having positive sweep near the endwalls, at an inlet flow angle of 37 deg, being close to the design incidence of 39 deg. The straight and swept case study cascades are labelled as STR and SWF in [2], respectively. These labels are used in the present paper as well. Sweep is said to be positive when

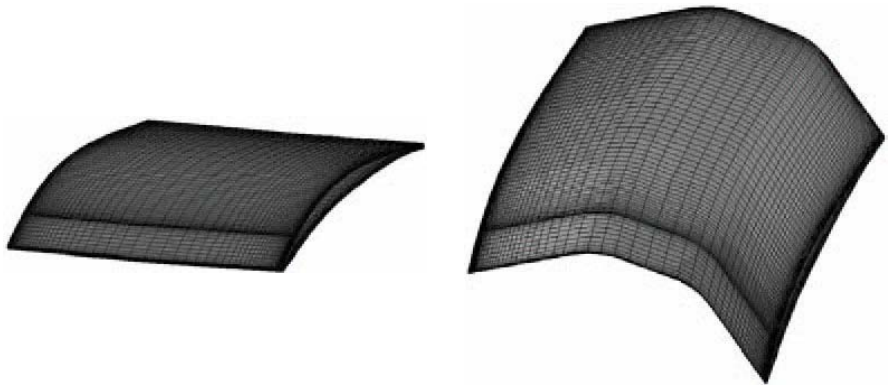

Fig. 1. STR (left) and SWF (right) blades [15]

a blade section under consideration is upstream of the adjacent inboard section [5]. Typical views of STR and SWF blades are presented in *Fig. 1*.

[17] offers measurement data on cascades of straight blades, in the midspan region of the central blade, for inlet flow angles from 24.5 deg up to 46 deg.

Fig. 2 shows a comparison of measured blade surface static pressure distributions at midspan of the central blades of cascades in [2] and [17] at near-design incidence: 37 deg for [2] and 39 deg for [17]. These are the only comparable detailed data sets in the two references. The static pressure is presented in terms of the static pressure coefficient

$$C_p = (p - p_1)/(\rho v_1^2/2) \tag{1}$$

where p is the local static pressure, and p_1 and v_1 are the mean static pressure and velocity at the inlet at midspan. The agreement appears to be 'reasonably good', as the 'visual inspection' of *Fig. 2* suggests. In order to get rid of subjectivity and to provide a quantitative indicator of agreement as well, the lift coefficient of the elemental blade section under consideration has been introduced. The definition of lift or drag coefficients is

$$C_{L,D} = \mathrm{d}F_{L,D}/(c\mathrm{d}S\rho v_\infty^2/2) \tag{2}$$

where dF is the aerodynamic force acting on the elemental blade section, and the indices L or D denote lift or drag forces (elemental force components acting normal to or parallel to the free-stream velocity), respectively.

C_L was approximated by means of numerical integration of the measured static pressure data over the blade surface at midspan. For the data out of [17] in *Fig. 2*, C_L has been estimated to 0.580 and was found 6 percent higher than C_L for the data out of [2]. The excess of lift could be due to the higher aspect ratio – leading to moderation of three-dimensional (3D) effects at midspan (see *Table 5* later on) – and higher Reynolds number in the case of [17]. However, based on *Fig. 8* being presented later on, the dominant portion of 6 percent excess in lift must

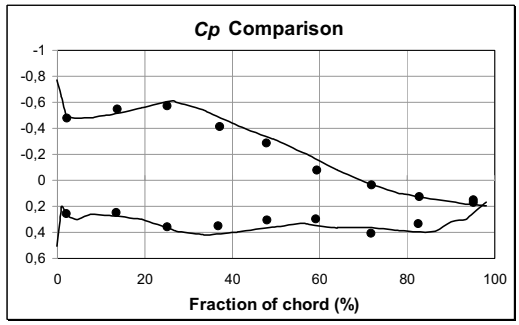

Fig. 2. Comparison of measured blade surface pressures at near-design incidence. Dots: [2], solid lines: [17]

just be due to the incidence angle being 2 deg higher in [17] than 37 deg in [2]. Considering these fact, the comparison of lift coefficient data confirmed the authors in the consistency of database formed by [2] and [17] despite the discrepancy of data in *Table 1*.

Table 1. Comparative cascade geometrical data and flow conditions

	[2]	[17]
Stagger angle, deg (from axial direction)	14.4	14.3
Solidity *c/s*	1.67	1.67
Aspect ratio *S/c*	1.27	2
Reynolds number	350.000	> 474.000

The experimental validation procedure was planned to consist of the following steps, after elaboration of the required CFD technique:

A/ Measurement data in [2] are to be compared with the related CFD results. The aim of this work is to confirm that the CFD tool represents quantitatively the cascade aerodynamics at a given (near-design) incidence, and the trends due to presence of endwall and due to sweep are resolved by the CFD tool at a reassuring level of significance.

B/ The thorough investigation of the effect of various flow incidences using 3D CFD models would have required months of CPU time at the level of computational infrastructure available at the time of studies presented herein. Thus, a reasonable compromise for CFD modelling simplification became unavoidable. The following considerations were made. The measurements at blade midspan in [17] were carried out on straight blades. Considering the relatively high aspect ratio for [17], the flow at midspan of the straight blades was presumed to be close to two-dimensional (2D).

If the results supplied at midspan by the already validated 3D model (see point A/) are in reasonably good agreement with those supplied by a suitable 2D CFD model, then the investigation for various flow inlet angles can be carried out by the use of the 2D model. This would reduce the CPU time to days. Therefore, the next step of the validation process would be the representative comparison of computed 3D and 2D results obtained at midspan.

C/ If the reduction of the CFD model from 3D to 2D is proven to be reasonable regarding the blade midspan region, the incidence-dependent 2D CFD data are to be compared to experimental results in [17].

3. CFD Technique

This paper has been written in accordance with the instructions in [19], formulating the requirements for analysis, validation and documentation of industry-related CFD tools.

For the CFD studies presented herein – based on cascade geometry in [2] –, the Reynolds number based on the inlet velocity, the blade chord and the kinematic viscosity of air at 20°C is 350.000. The Mach number computed with the inlet velocity and the speed of sound in air at 20°C is 0.15 and therefore, the flow is considered incompressible in the computations.

The case studies have been simulated by means of the commercially available finite-volume CFD code FLUENT 6.1 [20]. GAMBIT has been used as the CAD software.

The turbulence model elaborated by Spalart and Allmaras [21] has been used, being accepted as giving good results for wall-bounded flows and boundary layers subjected to adverse pressure gradients. It has been recommended for use in advanced design systems of swept-bladed turbomachinery [8]. Stationary flow has been modelled.

The inlet velocity profile, used as inlet condition, has been established on the basis of [2]. The following inlet conditions were set: inlet turbulence intensity of 0.05, length scale of 0.01 m. The modified turbulent viscosity ratio, the transported variable of the Spalart-Allmaras model, was computed as the product of $(3/2)^{0.5}$ times the mean velocity, the turbulence intensity and the length scale. Extensive tests were carried out on the sensitivity of CFD results to the inlet condition. It was concluded that the lower the inlet turbulence intensity, the reduced the losses and the increased the lift along the entire blade span by the computations.

The computational domain includes one blade passage (repeating itself periodically in order to compose an infinite blade row), with one blade located in the middle of the pitch (blade spacing). Utilizing the feature of the cascade configuration, boundary condition of periodicity (based on the profile camber geometry) has been applied. A zero diffusion flux condition has been used for all flow variables at the cascade outlet (outflow condition in FLUENT [20]).

In a multi-step development process, a 2D grid has been elaborated and 2D

preliminary CFD tests were carried out first. The 2D computational domain of one blade passage, including the blade at mid-pitch, extends 1 chord upstream and 2 chords downstream of the blade. The refined grid in the vicinity of the blade of controlled diffusion profile, with enlarged views in the near-leading and -trailing edge (LE, TE) regions is presented in *Fig.3.a*. The 2D grid consists of approx. 16.000 quadrilateral cells. An O-type grid was used around the blade and an unstructured part around the O part, as can be seen in the figure. The total number of cells is 81 on both the suction (SS) and the pressure side (PS), and is 25 and 29 in the vicinity of the LE and TE, respectively.

The 2D grid skewness characteristics fulfil the requirements. The most skewed cells appear approx. 1/4 chord upstream and downstream of the blade at mid-pitch, as well as 1/4 chord downstream of the LE and 1/4 chord upstream of the TE on the SS. These cells make up 6.6 percent of the total number of cells and are characterized by still reassuring equiangle skew above 0.5. The equiangle skewness of a cell is defined as the maximum value of the ratio of actual and possibly highest deviation from the optimum angle, considering each vertex [20]. The equiangle skew of none of the cells exceeds the pessimistically established upper limit of 0.6.

The 2D grid is generally free from drastic jumps in cell size. The expansion ratio, i.e. ratio of edge-size of neighbouring elements in the near-blade region has been set in a range of 1.12 to 1.15, both along the blade contour and normal to it. The thickness of the cell layer closest to the blade surface is in the range of 0.004 to 0.007 percent chord.

The aspect ratio, i.e. the ratio between the blade contour-wise and normal-to-blade extension of the cells, is in the order of magnitude of 50 to 100 closest to the blade surface. Such high values were accepted for the boundary layer, according to the note in [19]. Farther away from the blade surface, the aspect ratio, i.e. the ratio of the sides of the elements is gradually reduced to the order of magnitude of 1.

In the 2D model, wall y^+ values are within the range of $0.1 \ldots 1.2$, what is appropriate for the low Reynolds number model.

2D grid sensitivity tests were carried out, by means of creating a refined grid with approx. 41.000 cells, applying refinement basically in the vicinity of the blade. Comparison of results for the two models showed practically no difference in the SS and PS static pressure distributions. Comparison of the velocity magnitude, the total pressure, and the turbulent viscosity data in the wake (at 8 percent chord downstream of the TE) indicated practically no difference, either.

The differential equations were solved segregated using single precision number representation. The discretization of the convective momentum and turbulent viscosity fluxes was carried out by the Second Order Upwind (SOU) method with the Total Variation Diminishing (TVD) slope limiter. The pressure in the momentum equation was interpolated using the Standard method of FLUENT [20]. The discretized set of equations was solved with a Gauss-Seidel algorithm accelerated by an algebraic Multigrid (AMG) method. The pressure-velocity coupling is the Simplec method [20].The proper convergence of the solutions was checked on the basis of the lift and drag forces on the blades as well as using the residuals of

the equations. The scaled residuals [20] decreased below 10^{-5} and 10^{-7} for the continuity and all the other equations, respectively.

The 3D grid structures were derived by extruding the 2D one along the stacking lines of both STR and SFW bladings. The skewness, expansion ratio, aspect ratio, and wall y^+ characteristics reported for the 2D model are typical for the 3D models as well. As an example, a grid for SWF is presented in *Fig.3.b*.

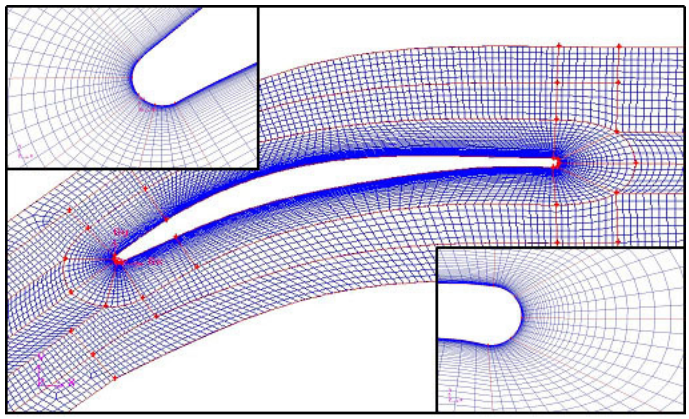

Fig. 3.a. Controlled diffusion blade profile and 2D computational grid [15]

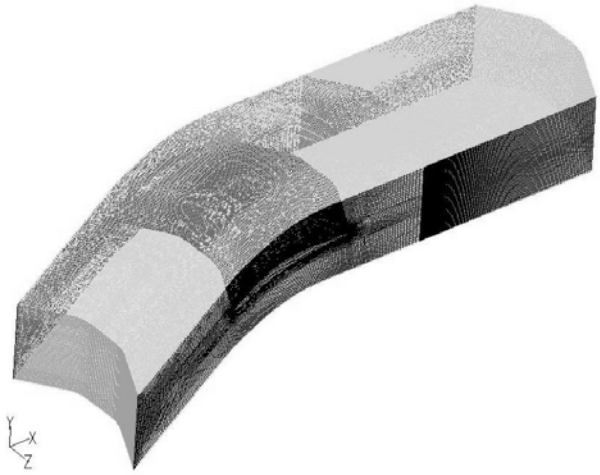

Fig. 3.b. Computational grid for SWF

Similarly to the methodology for the grid-dependence study in [13], a 3D 'mid-mesh' has been elaborated for reference purposes for both types of blades. 80 nodes have been used in the spanwise direction, resulting in a total number of approx. 1.200.000 cells. The expansion ratio along the half span is approx.

1.1, resulting in a symmetrically refined grid near the wall boundaries. 'Finer' and 'coarse' meshes [13] have also been generated for grid sensitivity studies, by means of doubling and halving the number of cells along the span and maintaining spanwise constant expansion ratio, but retaining the original 2D grid structure.

Table 2 summarizes the results of the grid dependence study. Following the basic guidelines in [13][15], the capability of the CFD tool has been characterized by means of quantitative indicators of C_L and C_D. These indicators have been judged the most representative in characterization of cascade aerodynamics [15]. C_L is greatly related to the static pressure distribution around the profile, whereas C_D is related to the CFD resolution of losses.

Similarly to the processing of data in *Fig. 2*, C_L was estimated by means of numerical integration of the measured static pressure data over the blade surface. The drag coefficient C_D (*Eq.*2) was derived with knowledge of the computed total pressure losses downstream of the blade passage, using the momentum equation, with assumption that the drag develops due to the total pressure loss compared to the inlet section, and with numerical integration of the outlet total pressure loss distribution along the pitch. Further details are given in [15]. These calculation methods for C_L and C_D will also be used further on.

Fitting to the database in [2] for further evaluation, C_L and C_D data were computed for two spanwise positions. Labels 'Midspan' and 'Near-endwall' denote data obtained at 50 and 4.7 percent span, respectively.

Table 2 shows the difference of C_L and C_D data obtained with use of the coarse and finer meshes relative to those obtained with use of the reference mid-mesh, at midspan and near the endwall, for both STR and SWF. The relative difference was calculated as the data under consideration minus the reference data, divided by the reference data.

The relative discrepancy in the lift coefficients is below 1 %. The relative discrepancy values of lift are lower for the finer mesh in most cases, indicating that further refinement of the mid-mesh does not lead to significant modification of the CFD tool from the aspect of lift computation.

Table 2. Results of grid sensitivity study

	STR			
	Rel. diff. in C_L		Rel. diff. in C_D	
	Coarse mesh	Finer mesh	Coarse mesh	Finer mesh
Midspan	− 0.3 %	− 0.2 %	0 %	0 %
Near-endwall	− 0.4 %	0 %	− 0.3 %	0.8 %

The CFD tool appears to be insensitive to mesh modifications from the viewpoint of representation of losses (and the related C_D values) at midspan. In *Table 2*, the maximum discrepancies can be observed in the drag coefficient values near the endwall, especially in the SWF case. During validation of the CFD tool and

its future application, special attention must be paid to this observation. Relative changes in C_D due to loss-reducing effects indicated by CFD near the endwall due to sweep are to be taken significant only if they exceed considerably the discrepancies in *Table 2*, i.e. if they dominate over the 'masking' effect of grid dependence.

The discrepancy data in *Table 2* are considerably lower than the uncertainty of measurement data being used for validation and presented in the next chapter.

Based on the above, the mid-mesh has been selected for the validation presented herein as well as for future applications, being considered as a mesh affected only moderately by grid dependence effects, and offering an economical CFD tool in terms of CPU time.

4. Experimental Validation

4.1. Validation Related to STR and SWF Blades at a Given Incidence

The measurement data presented in this section were taken directly or indirectly from the diagrams in [2]. *Fig.4* presents the comparative measured and computed static pressure coefficients C_p (*Eq.* 1) on the SS and PS. *Fig. 5* shows plots of measured and computed total pressure loss coefficients ω in a plane parallel to the pitchwise direction at 98 percent chord, starting from the SS (zero fraction of pitch).

$$\omega = (p_t - p_{t1})/(\rho v_1^2/2) \tag{3}$$

where p_t is the local total pressure and p_{t1} is the mean total pressure at the inlet at midspan.

A careless CFD 'validation' may appear as presenting comparative diagrams of arbitrarily selected CFD and experimental data without further quantitative discussion. Instead, it is essential to quantify the comparison. The 'visual' comparison of experimental and CFD data in *Fig. 4* shows a generally 'good' agreement. The sparseness of midspan measurement data points in *Fig.5* is due to the limited spatial resolution of data published in [2]. As *Fig. 5* suggests, the CFD model overestimates the thickness of the high-loss zone including the blade boundary layer, but the trend of measured loss profiles is represented well by the numerical model.

In order to provide a quantitative comparison, C_L and C_D were computed using the experimental as well as CFD data. Comparison of measurement- and CFD-based data of C_L and C_D reflects in a synthetic manner to what extent can the CFD tool resolve inviscid and viscous effects, respectively. C_L was calculated by means of numerical integration of the static pressure over the blade surface, using the experimental as well as CFD data in the surface points where static pressure measurements were carried out. C_D was derived as specified in the comments related to *Table 2*. It is obvious that the above calculation methods are approximate, however, they were consequently applied to both the measured and CFD results, thus providing comparative data. The measurement- and computation-based C_L and C_D as well as their relative discrepancy are presented in *Table 3*. Absence of

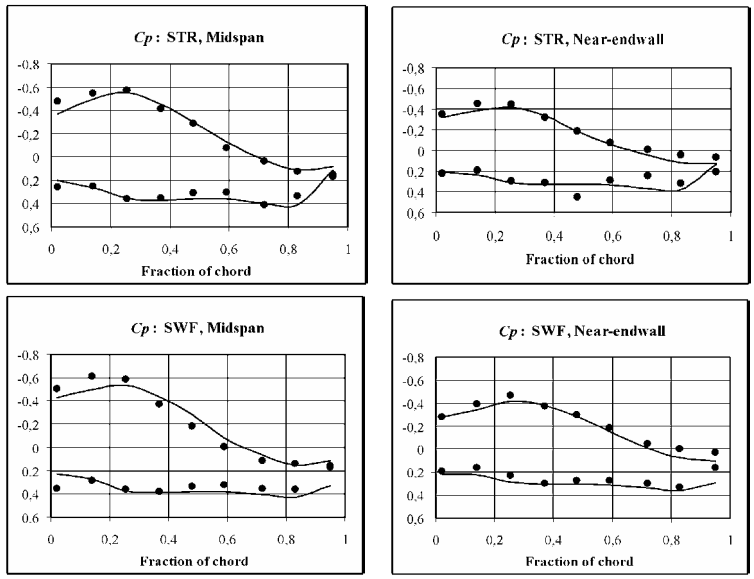

Fig. 4. Comparison of C_p surface static pressure coefficient data. Dots: measurement data from [2], solid lines: CFD

C_{Dm} data in the table is due to the insufficient spatial resolution of measured ω values at midspan to calculate the drag coefficient. The experimental uncertainty of both *Cp* and ω is pessimistically estimated as $\pm$ 0.003 [2]. The uncertainty for C_{Lm} and C_{Dm} are estimated as $\pm$ 0.006 and $\pm$ 0.003, respectively. It must be emphasized here that the relative discrepancies of C_L and C_D in *Table 2* due to grid dependency and in *Table 3* due to modelling uncertainty are within the range of experimental uncertainty, except for the C_L data at midspan in *Table 3*.

The data in *Table 3* indicate a reasonably good agreement between experiments and computations, being especially good in the near-endwall zone. Beside this quantitative comparison, the applicability of the CFD tool in design and optimization is to be judged on the basis of its capability to resolve the significant trends indicated by the measurements. The most characteristic trends (changes) which are indicated by the experiments in [2] and can be quantified with use of the local C_L and C_D data (using *Table 3*) are listed in *Table 4*. The trends are quantified in the table with use of relative changes, for the experiments as well as for the CFD results. The data indicate that the CFD methodology is capable of resolving the trends appearing in the measurements. The relative changes predicted by CFD are considerably higher than data in *Tables 2* and *3*. Therefore, it is established that the related physical phenomena – which will be of great significance in future applications – are definitely resolved by the CFD tool despite the 'masking' effects of grid dependence (conf. *Table 2*) and modelling uncertainty (conf. *Table 3*).

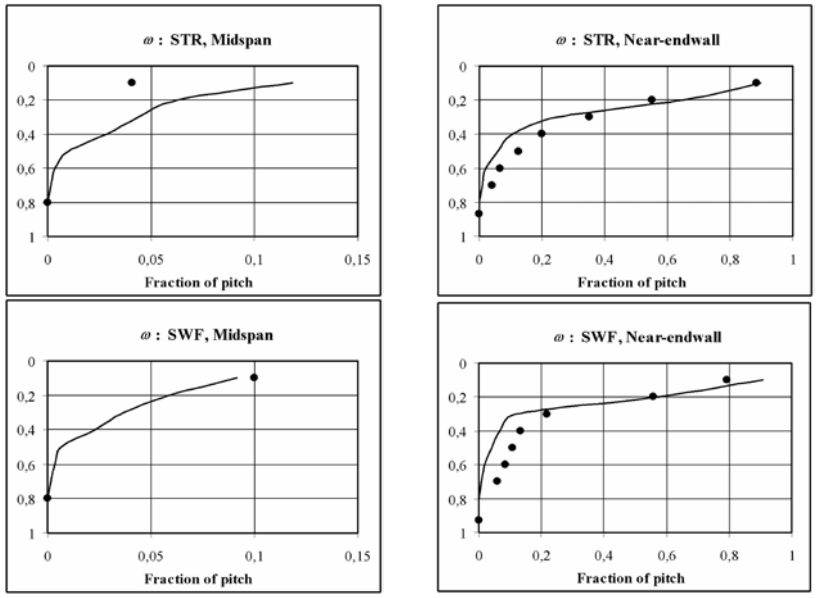

Fig. 5. Comparison of ω total pressure loss coefficient data. Dots: measurement data from [2], solid lines: CFD

The capability of the CFD tool to resolve 3D flow phenomena, involving loss-generating effects such as 3D separation [22] including corner stall, is demonstrated in *Fig. 6*. The figure shows computed ω = 0.6 iso-surfaces for the two bladings. The shape and dimensions of the experimentally determined stall zones [2] as well as the shrinkage of the corner stall zone due to the loss-reducing effect of positive sweep near the endwall are properly represented by the computations.

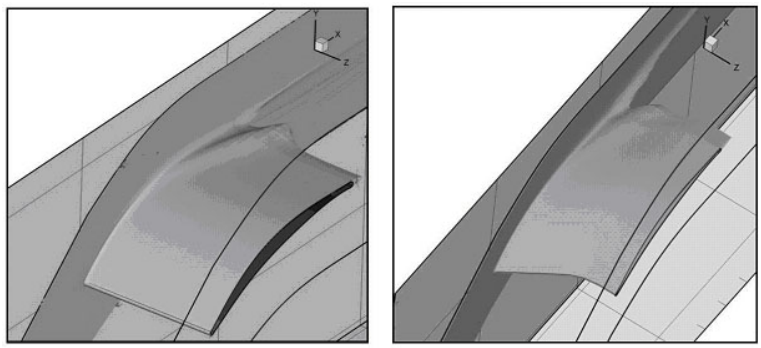

Fig. 6. Computed ω= 0.6 iso-surfaces. Left: STR, right: SWF.

Table 3. Comparative experiment – and CFD-based data

	STR		SWF	
	Midspan	Near-endwall	Midspan	Near-endwall
C_{Lm}	0.544	0.480	0.535	0.480
C_{Lc}	0.581	0.476	0.570	0.481
$\lvert\Delta C_L/C_{Lm}\rvert$	6.8 %	0.8 %	6.5 %	0.2 %
C_{Dm}	-	0.0800	-	0.0714
C_{Dc}	0.0175	0.0797	0.0189	0.0735
$\lvert\Delta C_D/C_{Dm}\rvert$	–	0.4 %	-	2.9 %

Table 4. Comparison of measured and computed trends

Trend	Relative change: experiments	Relative change: CFD
Reduction of C_L near the endwall compared to the midspan value, for STR	12 % reduction (0.544-0.480)/0.544	18 % reduction (0.581-0.476)/0.581
Reduction of C_L near the endwall compared to the midspan value, for SWF	10 % reduction (0.535-0.480)/0.535	16 % reduction (0.570-0.481)/0.570
Reduction of C_D near the endwall of SWF compared to the near-endwall value for STR, due to the loss-reducing effect of positive sweep	11 % reduction (0.0800-0.0714)/0.0800	8 % reduction (0.0797-0.0735)/0.0797
Increase of C_D at midspan of SWF compared to the midspan value for STR	Increase reported qualitatively in [2]	8 % increase (0.0189-0.0175)/0.0175

4.2. Comparison of 3D CFD Results at Midspan with 2D CFD Results

Table 5 compares the CFD-based C_L and C_D data obtained with use of the 3D STR model at midspan as well as using the 2D model described in Chapter 3, at flow incidence angle of 37 deg. The relative discrepancies were calculated as the 2D data under consideration minus the 3D data, divided by the 3D data. The 2D computations supply results of increased lift and reduced drag. This is in agreement with the classic view formulated in [23] that the approximation of 2D cascade flow is beneficial from the viewpoint of turbomachinery performance and efficiency improvement. Despite the observation of discrepancies, they are judged to be sufficiently low to test the capability of the CFD methodology to resolve the effects of variable incidences with use of the 2D model, via comparison of 2D CFD results with the experimental data in [17]. This validation procedure is presented

in the following section. Attention must be paid to the ‘masking’ effect due to the 2D-3D CFD discrepancy during experimental validation.

Table 5. Comparative computational STR 3D midspan and 2D data

	STR 3D, midspan	**2D**
C_{Lc}	0.581	0.600
Relative discrepancy in C_{Lc}	**3.3 %** (0.600-0.581)/0.581	
C_{Dc}	0.0175	0.0166
Relative discrepancy in C_{Dc}	**− 5.1 %** (0.0166-0.0175)/0.0175	

4.3. Validation of the CFD Method Regarding Resolution of Incidence-dependent Effects

Fig. 7 presents the comparison of measurement-based distribution of blade surface C_p data at midspan, reported in [17], with the 2D CFD results, at three representative incidences. The visual comparison suggests that the agreement is generally ‘good’, even at the highest incidence at which the nearly constant C_p values close to the TE of the SS indicate the presence of a separation zone. The CFD model underestimates the SS depression at the incidence angle of 33 deg. The reason is to be studied in the future.

C_L lift coefficients were calculated from both experimental [17] and CFD data and are presented in *Fig. 8*. The experiment-based trends are followed properly by the computations, i.e. the computed lift increases with the incidence at the slope suggested by the measurements, and nearly constant C_L is predicted beyond the incidence of 37 deg. The computation overestimates the lift, which must be predominantly due to the 2D-3D CFD discrepancy discussed in the previous section. An exception is the 33 deg incidence case, which is probably due to the CFD underestimation of SS depression reported in *Fig. 7*. By the way, the experimental data point related to 33 deg incidence appears to misfit the measured trends.

In order to investigate the effect of incidence on losses, the definition of overall total pressure loss must be introduced, fitting to the evaluation process in [17]:

$$\bar{\omega} = \frac{\overline{p}_{t1} - \overline{p}_{t2}}{\overline{p}_{t1} - \overline{p}_{1}} \tag{4}$$

Mass-averaging means mass-averaging over the entire blade passage cross-section in the 3D case, whereas it means mass-averaging of quantities related to a cascade section of infinitely small thickness in the 2D case. Since 3D effects,

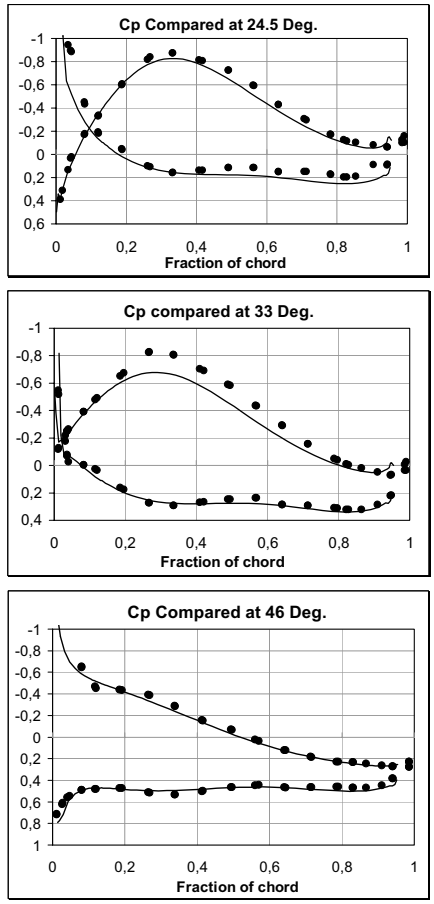

Fig. 7. Effect of changing incidence on the blade surface static pressure coefficient C_p. Dots: measurement data from [17], solid lines: 2D CFD

mainly governed by the presence of endwalls, play important role in mass-averaging in the 3D case, significant discrepancy occurs between the measurement-based 3D and the CFD-based 2D $\bar{\omega}$ data. In order to make possible a comparison between experimental and CFD data despite this discrepancy, the following data processing was carried out. For both experimental and CFD data, the C_L results of *Fig. 8* were divided by the corresponding $\bar{\omega}$ data computed on the basis of *Eq.* (1), and the resultant data sets were normalized by the maximum C_L / $\bar{\omega}$ values. The results are presented in . The experiment-based data in *Fig. 9* are below the *Fig. 9*. CFD-based ones, representing the increased effect of 3D (also endwall) phenomena reducing the lift-to-loss ratio at incidences considerably lower or higher than the mean value

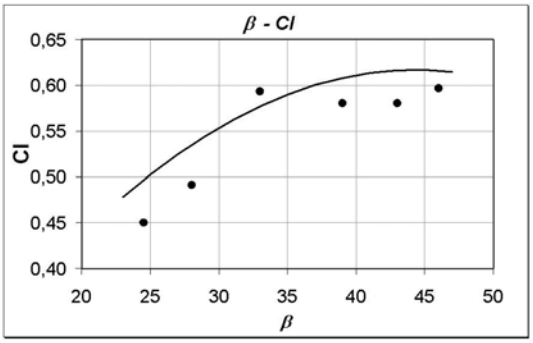

Fig. 8. Dependence of C_L on the incidence angle β. Dots: data based on measurement results in [17], solid line: 2D CFD

in the incidence angle range. Both the experiment- and CFD-based diagrams give a maximum lift-to-loss ratio at nearly the same incidence angle of 35 deg. The lift-to-loss ratio presented in the figure is in analogy to the lift-to-drag ratio of airfoil sections. Obtainment of maximum blade section lift-to-drag ratio is a means of turbomachinery efficiency improvement [7, 15]. Therefore, reliable prediction of the optimum incidence angle is an important feature of the CFD tool presented herein from the aspect of its future application in turbomachinery design and optimization.

The experimental uncertainty of Cp and C_{Lm} for [17] is estimated to be equal as for [2], and the uncertainty of $\bar{\omega}$ for [17] is estimated to be equal to that of ω for [2].

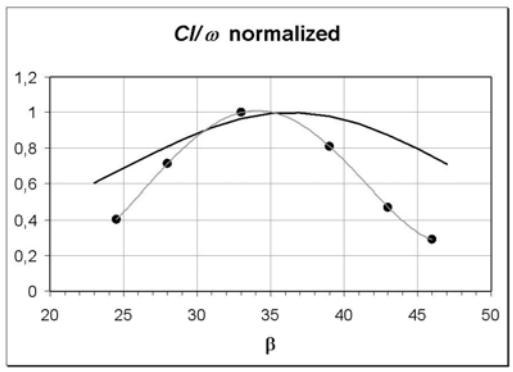

Fig. 9. Comparison of normalized $C_L/\bar{\omega}$ diagrams. Dots: data based on measurement results in [17], solid line: 2D CFD

5. Summary

Elaboration and experimental validation of a CFD technique for stationary linear cascades has been presented herein. With introduction of suitably prescribed sweep and stagger angle distributions along the span, this CFD technique will be used by the authors in the future, filling the gap in CFD investigation and optimization of axial flow cascades of twisted-swept blades.

The CFD methodology has been thoroughly documented in accordance with the requirements regarding industrial CFD tools. The documentation includes reporting on the following items: cascade geometry; the applied turbulence model; the inlet boundary conditions and the sensitivity of the CFD results to their prescription; outlet boundary condition; the further boundary conditions; the computational domain and grid structure; grid quality including data on cell skewness, expansion ratio and aspect ratio; wall y^+ values; details on the computation methodology; convergence characteristics; and detailed grid dependence studies showing favourable results.

The experimental validation procedure has been carried out on a strict quantitative basis. It indicated that at near-design incidence, the CFD technique predicts the aerodynamic lift and drag characteristics at accuracy reasonably high from engineering point of view, for both straight and swept blades. The accuracy is especially high near the endwalls where sweep finds wide application in order to modify the blade aerodynamics in a favourable manner. The trends measured at near-design incidence – reduced lift near the endwalls, and reduced endwall and increased midspan losses due to positive sweep – have been properly resolved by the CFD technique. The CFD method well reproduces the experimentally detected 3D flow features such as corner stall, in terms of shape as well as dimensions of the stall zone. In accordance with the experiments, the moderation of corner stall zone due to the beneficial effect of positive sweep near the endwall is indicated by the CFD prediction.

The CFD tool represents well the measured quantitative characteristics of incidence-dependent lift in the case of straight-bladed cascades. These characteristics are: slope of the C_L – incidence angle curve, and a nearly horizontal plateau of this curve above incidences of 37 deg, in the incidence range under investigation. The CFD technique predicts well the incidence angle at which the measurements indicate a maximum ratio between the blade performance (lift) and total pressure losses.

Based on the validation, authors consider the presented CFD technique reliable to be used as a basis in future prediction of aerodynamics of twisted-swept blades.

Acknowledgements

This work has been supported by the Hungarian National Fund for Science and Research under contracts No. OTKA T 043493 as well as No. OTKA T 037651, and, on the behalf of J. Vad, out of the István Széchenyi Fellowship under contract No. SZÖ 271/2003.

Symbols

$C[-]$	force coefficient (lift, drag)
$C_p[-]$	static pressure coefficient
$c[m]$	blade chord
$dF\ [N]$	elemental force
$p[Pa]$	local static pressure
$p_t[Pa]$	local total pressure
S[m]	blade span (height)
s[m]	blade spacing (pitch)
v[m/s]	fluid velocity
$y^+[-]$	wall normal cell size (in wall units)
β [deg]	flow incidence angle (measured from axial direction)
Δ	discrepancy (CFD and measurement data)
ρ [kg/m^3]	fluid density
ω [-]	local total pressure loss coefficient (*Eq.* 3)
$\bar{\omega}$[-]	overall total pressure loss coefficient (*Eq.* 4)

Subscripts and Superscripts

c	CFD-based
D	drag
L	lift
m	measurement-based
1	cascade inlet
2	cascade outlet
∞	free-stream characteristics
	mass-averaged value

References

[1] SHANG, E.– WANG, Z. Q. – SU, J. X. (1993), The Experimental Investigations on the Compressor Cascades with Leaned and Curved Blade, ASME paper No. 93-GT-50.

[2] SASAKI, T. – BREUGELMANS, F. (1998), Comparison of Sweep and Dihedral Effects on Compressor Cascade Performance, ASME J Turbomachinery, **20**, pp. 454–464.

[3] SONG, Y.– ZHAO, G.– CHEN, F.– WANG, Z., Experimental Study of Sweep and Dihedral Effects on Compressor Cascade Performance, *Proc. 6th European Conference Turbomachinery Fluid Dynamics and Thermodynamics, Lille, France*, (2005) pp. 1–9.
[4] BOGERS, P., Investigation of the Effects of Sweep and Dihedral on the Development of Compressor Blade Secondary Losses, *Project Report 1997-23, Von Karman Institute for Fluid Dynamics* (1997).
[5] CLEMEN, C. – STARK, U. (2003), Compressor Blades with Sweep and Dihedral: a Parameter Study, *Proc. 5th European Conference Turbomachinery Fluid Dynamics and Thermodynamics*, Prague, Czech Republic, pp. 151–161.
[6] BEILER, M. G.– CAROLUS T. H. , *Computation and Measurement of the Flow in Axial Flow Fans With Skewed Blades*, ASME J Turbomachinery, **121**, (1999) pp. 59–66.
[7] VAD, J.– KWEDIKHA, A. R. A.– JABERG, H., Influence of Blade Sweep on the Energetic Behavior of Axial Flow Turbomachinery Rotors at Design Flow Rate, ASME Paper GT2004-53544 (2004).
[8] GALLIMORE, S. J.– BOLGER, J. J.– CUMPSTY, N. A.– TAYLOR, M. J.– WRIGHT, P. I. – PLACE, J. M. M., The Use of Sweep and Dihedral in Multistage Axial Flow Compressor Blading – Parts I and II. ASME J Turbomachinery, **124** (2002) pp. 521–541.
[9] KUHN, K., Experimentelle Untersuchung einer Axialpumpe und Rohrturbine mit gepfeilten Schaufeln, Ph.D. Thesis, Technische Universität Graz, Institut for Hydraulische Strömungsmaschinen, (2000).
[10] United States Patent (2002), *High Efficiency and Low Weight Axial Flow Fan*, Patent No. US 6,368,061 B1.
[11] MOREAU, S., HENNER, M., – NEAL, D., 3D Rotor-Stator Interaction in Automotive Engine Cooling Fan Systems, *Proc. 6th European Conference Turbomachinery Fluid Dynamics and Thermodynamics, Lille, France*, (2005) pp. 145–157.
[12] VAD, J.– KWEDIKHA, A. R. A.– KRISTÓF, G.– LOHÁSZ, M. M.– RÁBAI, G.– RÁCZ, N. – WATANABE, K. Effects of Blade Skew in an Axial Flow Rotor of Controlled Vortex Design, *Proc. 6th European Conference Turbomachinery Fluid Dynamics and Thermodynamics, Lille, France* , (2005), pp. 46–55.
[13] CORSINI, A, RISPOLI, F. (2004), Using Sweep to Extend the Stall-Free Operational Range in Axial Fan Rotors, *Proc. of IMechE, Part A – Journal of Power and Energy*, **218**, pp. 129–139.
[14] YAMAGUCHI, N. – TOMINAGA, T.– HATTORI, S. – MITSUHASHI, T., Secondary-Loss Reduction by Forward-Skewing of Axial Compressor Rotor Blading, *Proc. Yokohama International Gas Turbine Congress, Yokohama, Japan*, (1991) pp. II.61-II.68.
[15] VAD, J. – LOHÁSZ, M. M. – RÁBAI, G. – RÁCZ, N. – TAJTI, Á. – VASSATIS, A. – CORSINI, A. , A Synthetic Method for Judging the Validity of a CFD Tool Applied to Axial Flow Cascades, *Proc. 6th European Conference Turbomachinery Fluid Dynamics and Thermodynamics, Lille, France*, (2005) pp. 10–19.
[16] BREUGELMANS, F., Experimental Investigation of Sweep and Dihedral in Compressors, in Turbomachinery Blade Design Systems, Lecture Series 1999-02, Von Karman Institute for Fluid Dynamics, (1999).
[17] SANGER, N. L. – SHREEVE, R. P.,Comparison of the Calculated and Experimental Cascade Performance for Controlled-Diffusion Compressor Stator Blading, *ASME J Turbomachinery*, **108**, (1986), pp. 42–50.
[18] SANGER, N. L. (1983), The Use of Optimization Techniques to Design Controlled-Diffusion Compressor Blading, *ASME J Engineering Power*, **105**, pp. 256–264.
[19] CASEY, M. – WINTERGERSTE, T. (editors), Best Practice Guidelines, ERCOFTAC Special Interest Group on 'Quality and Trust in Industrial CFD', Version 1.0, January 2000.
[20] FLUENT 6.1 User's Guide, (2003), Fluent Inc., Lebanon, NH, USA.
[21] SPALART, P.– ALLMARAS, S. (1992), A One-Equation Turbulence Model for Aerodynamic Flows, *AIAA Technical Report AIAA-92-0439*.
[22] GBADEBO, S. A. – CUMPSTY, N. A. – HYNES, T. P. (2005), Three-Dimensional Separations in Axial Compressors, *ASME J Turbomachinery*, **127**, pp. 331–339.
[23] BREUGELMANS, F. A. E., Energy Efficient Design through Fluid Dynamics Improvements in Turbocomponents. *International Seminar on Thermal and Fluid Engineering for Advanced Energy Systems* Institute of Advanced Material Study, Kyushu University, Kasuga, Japan,(1997).